

Quantum Suppression of the Rayleigh Instability in Nanowires

F. Kassubek,^{1,2} C. A. Stafford,² Hermann Grabert,¹ and Raymond E. Goldstein^{2,3}

¹*Fakultät für Physik, Albert-Ludwigs-Universität, Hermann-Herder-Straße 3, D-79104 Freiburg, Germany*

²*Department of Physics and ³Program in Applied Mathematics, University of Arizona, Tucson, AZ 85721*

A linear stability analysis of metallic nanowires is performed in the free-electron model using quantum chaos techniques. It is found that the classical instability of a long wire under surface tension can be completely suppressed by electronic shell effects, leading to stable cylindrical configurations whose electrical conductance is a magic number 1, 3, 5, 6,... times the quantum of conductance. Our results are quantitatively consistent with recent experiments with alkali metal nanowires.

Plateau's celebrated study [1,2] of the stability of bodies under the influence of surface tension established a fundamental result of classical continuum mechanics: a cylinder longer than its circumference is energetically unstable to breakup. Here we consider a quantum mechanical generalization of Plateau's study—the stability of a metallic nanowire. Methods from the study of quantum chaos are used to examine the energetics of a free electron gas in a jellium filament, and show that an infinite filament can be stable against all axisymmetric perturbations if its electrical conductance G [in units of $G_0 = 2e^2/h = (12,906.4 \text{ Ohm})^{-1}$] belongs to a set of "magic numbers" $n = 1, 3, 5, 6, \dots$ and is otherwise unstable. Here e is the charge of an electron and h is Planck's constant. Such magic numbers are analogous to those found in the shell model of atomic nuclei [3] and in metal clusters [3,4]. Our stability analysis elucidates and confirms the stability properties of simple metal nanowires conjectured by Yanson, Yanson, and van Ruitenbeek [5] based on their observation of shell structure in the conductance statistics of sodium nanowires.

Structural multistability of metallic nanowires was previously postulated based on classical molecular dynamics simulations [6–8]. However, the magic numbers observed in conductance histograms in alkali metals [5,9] are clearly an electronic shell effect, as shown below, and cannot be explained with classical molecular dynamics. The common occurrence of multistability in two such radically different models likely stems from the fact that both models introduce an additional length scale (the Fermi wavelength λ_F in the free electron model, the atomic diameter in molecular dynamics simulations), which leads to commensurability effects.

The properties of nanowires formed from simple monovalent metals, like the bulk properties of these materials [10], are determined largely by the delocalized conduction electrons. A free electron jellium model, treating the electrons as a noninteracting Fermi gas confined within

the wire by hard-wall boundary conditions, provides an intuitive and even quantitative explanation of observed quantities like force and conductance [11–13].

To examine energetic stability, we treat the full quantum mechanics of an ideal electron gas in a weakly deformed cylinder, and find its thermodynamic potential to quadratic order in the amplitude of the deformation. A contribution proportional to the filament area, naturally identified as the surface tension, is only one of several competing terms in the free energy, which consists of terms which vary smoothly with the geometry of the filament and an oscillatory contribution directly connected with the discrete energy levels that are solutions to the Schrödinger equation. The smooth terms appear in descending powers of length (proportional to volume, surface area, mean curvature, etc.), and are quite analogous to those found in the study of classical wave equations in curved domains [14] and the related problem of classically screened Coulomb (Debye-Hückel) interactions of curved surfaces in an electrolyte [15]. The present work is thus fundamentally distinct from that which has dealt with the quantum mechanical origin of surface tension itself in metallic fluids [16], as well as those which consider quantum mechanical corrections to classical surface tension due to the quantization of capillary waves [17].

To be specific, we examine an infinite cylindrical wire and its sole classically unstable deformation—an axially symmetric one (see Fig. 1). Any such deformation can be written as a Fourier series:

$$R(z) = R_0 \left(1 + \int_0^\infty dq b(q) \cos(qz + \phi(q)) \right), \quad (1)$$

where $R(z)$ is the radius at position z , R_0 is the unperturbed radius, $b(q)$ is the (infinitesimal) perturbation coefficient, and $\phi(q)$ is an arbitrary phase shift. The coefficients $b(q)$ are chosen such that the total volume of the wire is unchanged by the deformation. Other physically reasonable constraints [13] are also possible, but lead to similar results.

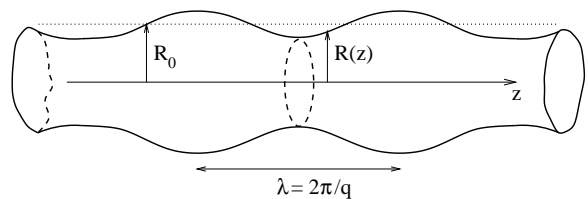


FIG. 1. Deformation of wavevector q of a cylindrical nanowire.

The metallic nanowire is an open system, connected to macroscopic metallic electrodes at each end [5,9,18–21]. Therefore the change of the grand canonical potential Ω under the perturbation determines its stability. Ω is related to the electronic density of states $g(E)$ by

$$\Omega = -k_B T \int_0^\infty dE g(E) \ln \left(1 + e^{-(E-\mu)/k_B T} \right), \quad (2)$$

where k_B is Boltzmann's constant, T is the temperature, and μ is the electronic chemical potential specified by the macroscopic electrodes. Our aim is to expand Ω up to second order in the coefficients $b(q)$ characterizing the deformation. As we will show, this yields

$$\Omega[b] = \Omega[0] + \int_0^\infty dq \alpha(q) [b(q)]^2 + \mathcal{O}(b^3). \quad (3)$$

The change in the grand canonical potential is of second order in b and contributions from deformations with different q decouple. If the prefactor $\alpha(q)$ is negative for any value of q , then Ω decreases under the deformation and the wire is unstable.

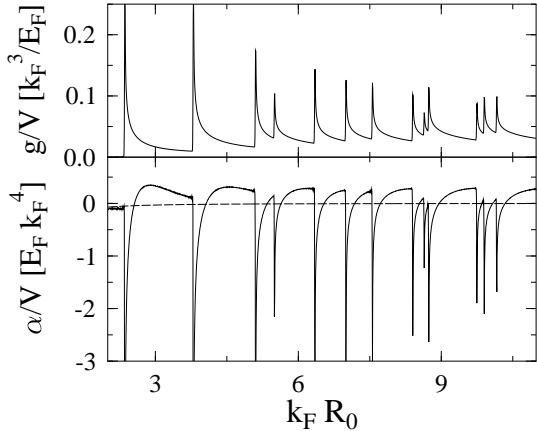


FIG. 2. Density of states $g(E_F)$ of a cylindrical wire (upper diagram) and stability coefficient α (lower diagram) versus the radius R_0 of the unperturbed wire. The wavevector of the perturbation is $qR_0 = 1$. Dashed curve: Weyl contribution to α .

For an infinite cylindrical wire, the transverse motion is quantized, leading to the formation of discrete electronic subbands. The total density of states is the sum of the contributions from each subband (see Fig. 2): every subband begins to contribute at a threshold energy equal to the energy of its quantized transverse motion with a sharp spike, falling off smoothly for increasing energy. If the Fermi energy E_F lies near one of these sharp peaks, certain small deformations of the wire can dramatically increase the density of states. According to (2), this lowers the grand canonical potential, leading to an instability. On the other hand, if there is no subband

threshold sufficiently close to E_F , the density of states will instead decrease with any deformation, implying the existence of stable regions intervening between the instabilities associated with the opening of each subband.

Quantum Chaos Approach

In order to examine this picture quantitatively, we use a semiclassical approach [3], which enables $g(E)$ to be split into a smooth average contribution $\bar{g}(E)$, referred to as the *Weyl contribution*, and an oscillatory part $\delta g(E)$, whose average value is zero. \bar{g} contains terms proportional to the volume of the nanowire, and to the area and curvature of its surface: $\bar{g}(E) = (1/E_F)\bar{g}(E/E_F)$, where

$$\bar{g}(x) = \frac{x^{1/2}}{2\pi^2} k_F^3 V - \frac{1}{8\pi} k_F^2 S + \frac{x^{-1/2}}{6\pi^2} k_F K, \quad (4)$$

and $k_F = 2\pi/\lambda_F$ is the Fermi wavevector. The volume V , surface area S , and integrated mean curvature K can be calculated for arbitrary perturbations by simple geometric considerations. The oscillatory part of the density of states is a quantum correction, and may be calculated in the semiclassical approximation as a sum over all periodic classical orbits of the system [3,12,13,22–24]:

$$\delta g(E) = \sum_{vw} A_{vw} \cos(S_{vw}/\hbar + \theta_v), \quad (5)$$

where v and w are defined in Fig. 3, A_{vw} is an amplitude depending on the stability, symmetry, and period of the orbit, S_{vw} is the classical action of the orbit, and θ_v is a quantum mechanical phase shift determined by the singular points and symmetry of the orbit. For free electrons, the action $S_{vw}/\hbar = k_F L_{vw}$, where L_{vw} is the length of the orbit. Each periodic orbit in a cylindrical wire lies in a plane transverse to the wire's axis, and there is a correspondence to the orbits [3] in a 2D circular billiard (see Fig. 3). To calculate the amplitudes of different orbits, we used the method described in [22].

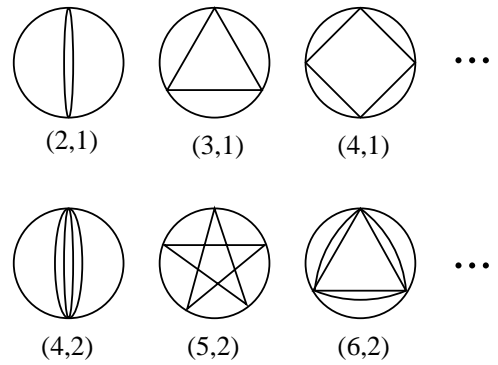


FIG. 3. Classical periodic orbits of an electron in a plane perpendicular to the z -axis, labeled (v,w) , where v is the number of vertices and w the winding number.

When the wire is deformed, the translational symmetry is broken, and we use a semiclassical perturbation theory [23,24] to calculate δg . This theory assumes that for small perturbations, the amplitudes and topology of the unperturbed orbits can still be used in (5), but that the lengths of the orbits—and hence their actions—change. The cosine in (5) is replaced by the average of the real part of $e^{i(S+\delta S)/\hbar+i\theta}$ over the measure of the broken symmetry group, where δS is the change of the action in first order. Combining this result for δg with (4), it is straightforward to calculate the density of states up to second order in the coefficients b for a deformed wire. The result can be integrated to obtain the grand canonical potential, which indeed has the expansion (3).

Stability Analysis

Let us first discuss the stability of a nanowire at zero temperature. Fig. 2 shows the stability coefficient α (lower diagram) and the density of states at the Fermi energy (upper diagram) as functions of the radius of the unperturbed wire. The wavelength of the perturbation was taken to be $qR_0 = 1$, the critical wavelength for stability in Plateau's classical analysis of a body under the influence of surface tension. In addition to surface tension, the present model for Ω has a curvature energy, which enhances the instability for small R_0 , and an oscillatory component associated with the opening of successive subbands as R_0 increases. As discussed above, α has sharp negative peaks—indicating strong instabilities—at the subband thresholds, where the density of states is sharply peaked. Under surface tension and curvature energy alone (dashed curve in Fig. 2), the wire would be slightly unstable at the critical wavevector $qR_0 = 1$, since the curvature term is negative. However, the quantum correction is positive in the regions between the thresholds to open new subbands, *thus stabilizing the wire*. Since the oscillatory contribution to α is independent of q , we find that regions of stability persist for *arbitrarily long wavelength perturbations*, indicating that an infinitely long cylindrical wire is a true metastable state if the radius lies in one of the windows of stability.

With these results, we can construct the zero temperature stability diagram for the wire [see Fig. 4(a)]. In contrast to Plateau's classical stability analysis, an additional quantum length scale arises here, namely the Fermi wavelength λ_F . The stability problem is now determined by two dimensionless parameters: qR_0 and $k_F R_0$. In Fig. 4, regions of instability, where the coefficient $\alpha(q)$ is negative, are shaded grey, while the stable regions are shown in white. Note that many of the white regions of stability persist all the way down to $q = 0$. The *multistability* of the system, indicated by the alternating stable and unstable stripes, reflects commensurability effects between λ_F and R_0 .

We remark that in addition to the axially symmetric modes considered here, which are the sole unstable

modes in the classical limit, perturbations which break axial symmetry may also become unstable near the subband thresholds. However, these Jahn-Teller like modes are likely less unstable than the axisymmetric modes, and will not destroy the regions of stability shown in Fig. 4(a).

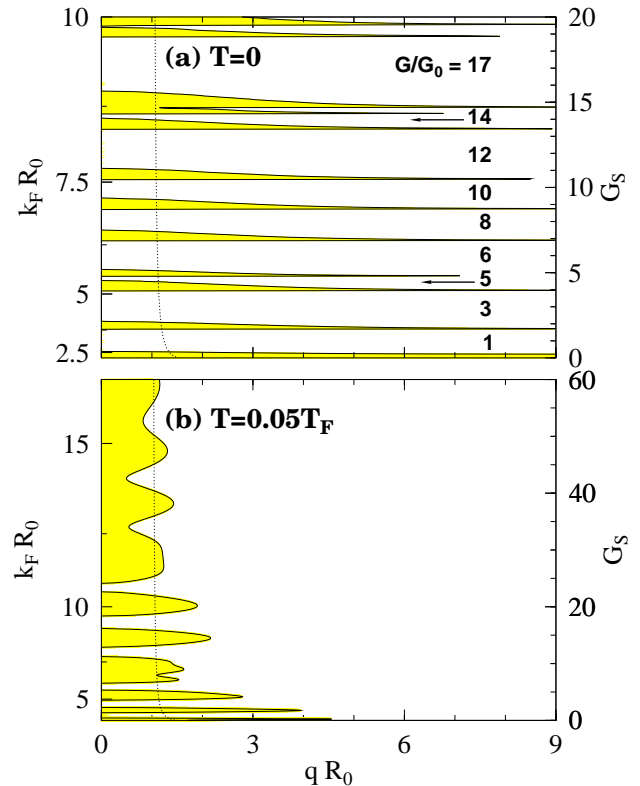


FIG. 4. Stability diagram for cylindrical nanowires at two different temperatures. White areas are stable, grey unstable to small perturbations. The quantized electrical conductance values G of the stable configurations are indicated by bold numerals in (a), with $G_0 = 2e^2/h$. Right vertical axis: corrected Sharvin conductance G_S . Dotted curve: stability criterion in the Weyl approximation.

Conductance Magic Numbers

The electrical conductance G of a perfect cylindrical nanowire is quantized [25] in units of $G_0 = 2e^2/h$. The quantized conductance values of the stable cylindrical configurations are indicated by bold numerals in Fig. 4(a). For comparison, the right vertical axis of the figure is labeled with the corrected Sharvin conductance [25]

$$G_S = \left(\frac{k_F R_0}{2} \right)^2 \left(1 - \frac{2}{k_F R_0} \right), \quad (6)$$

which gives a smooth approximation to G/G_0 . The conductance values of the stable configurations are somewhat analogous to the *magic numbers* of enhanced stability in atomic nuclei [3] and metal clusters [3,4]. An important distinction is that the magic numbers in nuclei and clusters refer to the number of fermions in a

finite system, while we consider an infinite, open system, with magic numbers describing the number of conducting transverse modes [11] which hold the wire together. The number of conducting modes is approximately equal to the number of atoms which fit within a cross section of the wire.

The integer magic numbers identified here are fundamentally different from the concept of “magic radii” proposed in [26,27]. The latter represented discrete minima of the energy per unit volume of a cylindrical jellium wire as a function of radius, but the stability with respect to changes in shape was not considered. A similar scenario for the free-electron model was advanced in Ref. [5] based on a partial summation of the periodic orbits in the expression for Ω itself. While the theoretical results of Refs. [5,26,27] may be suggestive, they have no direct relation to the systematic linear stability analysis performed here; in particular, the calculations of Refs. [5,26,27] appear to suggest that stability occurs only for a discrete set of radii, of measure zero, while our analysis finds stability with respect to all small perturbations over broad intervals of radius. Furthermore, the very existence of discrete energetic minima of the type discussed in Refs. [5,26,27] depends sensitively on the numerical value of the surface tension in the model; for example, they do not occur whatsoever in the free-electron model at constant volume for $G > G_0$. In contrast, the finite windows of stability in our analysis are robust with respect to variations of the surface tension.

Comparison to Experiments in Alkali Metals

The sequence of magic numbers $G/G_0 = 1, 3, 5, 6, \dots$ is consistent with the observation of conductance quantization in alkali metal point contacts [9]. Recently, conductance histograms for sodium nanowires with pronounced peaks up to $G/G_0 \sim 100$ were obtained by Yanson *et al.* [5]. They argued that these peaks could not be understood based on conductance quantization alone, but rather reflected energetically preferred wire configurations. In order to construct a theoretical conductance histogram, we need to know the *a priori* probability of occurrence of a nanowire of a given cross-sectional area. Here, we make the simplest hypothesis: that *nanowires of different cross-sectional areas occur with equal a priori probability if stable, and with zero probability otherwise*. On this hypothesis, the relative probability of observing a contact with a given quantized conductance value is proportional to the width ΔG_S of the corresponding stable region, G_S being a dimensionless measure of the contact area.

The conductance histogram from Ref. [5] taken at a temperature of $T = 80\text{K}$ is reproduced in our Fig. 5(a). For comparison, the theoretical magic numbers at the same temperature are plotted as vertical bars, with height equal to the width ΔG_S of the corresponding

stable region. Unlike the idealized wires in our analysis, the experimental wires are of finite length, and contain imperfections. Thus the peaks in the experimental histogram are shifted [28] below the theoretical integer values due to backscattering, and are broadened [28] due to tunneling, disorder-induced conductance fluctuations, and inelastic processes. Furthermore, the relative heights of the peaks may be influenced by dynamical as well as energetic effects; in particular, the peak at $G = G_0$, which is quite pronounced at the lowest temperatures [5,9], is absent from the experimental histogram at $T = 80\text{K}$ —presumably indicating that thermally activated processes lead to the rupture of this metastable configuration. For $G/G_0 > 50$, the experimental signal to noise ratio is probably not sufficient to resolve individual magic numbers. Nonetheless, the agreement between theory and experiment for $G/G_0 < 50$ is striking.

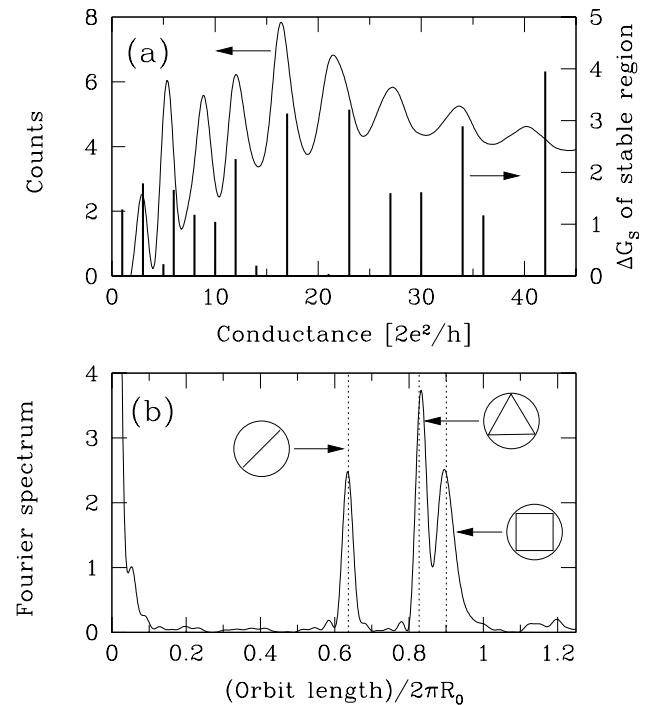


FIG. 5. Magic numbers: theory and experiment. (a) Solid curve: conductance histogram for sodium nanowires at $T = 80\text{K} = 0.002T_F$, reproduced from Ref. [5]. Vertical bars: quantized conductance values of the metastable nanowire configurations in the free electron model at the same temperature. The height of each bar is equal to the width ΔG_S of the corresponding stable region [c.f. Fig. 4(a)]. (b) Fourier power spectrum of the theoretical conductance histogram [vertical bars in (a)], displaying the dominant contributions of the three shortest periodic orbits in Eq. (5).

The widths of the stable regions vary in a nontrivial, quasiperiodic fashion as a function of the conductance, due to the interference of various periodic orbits in Eq. (5). The actions of the periodic orbits are proportional to

the radius of the wire, and hence are approximately proportional to the square root of the conductance, by Eq. (6). The contributions of the various periodic orbits to the conductance histogram can thus be extracted [29] by taking a Fourier transform with respect to $\sqrt{G/G_0}$. The Fourier power spectrum of the theoretical conductance histogram is shown in Fig. 5(b), where all magic numbers up to $G/G_0 = 207$ were included. It shows clear peaks corresponding to the three shortest periodic orbits, and is quantitatively consistent with the experimental Fourier spectrum for sodium nanowires obtained by Yanson *et al.* [29]. The experimental peaks [29] are broader than those in Fig. 5(b) since the oscillatory structure in the experimental histogram is damped for $G/G_0 > 50$.

It should be pointed out that a conductance histogram constructed under the assumption that *all* contact areas occur with equal likelihood (including unstable contacts) yields a Fourier spectrum in which the contributions of the three shortest periodic orbits have a form similar to that shown in Fig. 5(b), although their overall amplitude is reduced. Such a model is excluded on theoretical grounds, but cannot be ruled out based on comparison to the experimental Fourier spectrum [29] alone.

Classical Limit

At zero temperature, the pattern of stable regions separated by unstable stripes shown in Fig. 4(a) continues up to arbitrarily large radii. However, at any finite temperature T , the quantum oscillations in α are smoothed out, and the classical stability criterion $qR_0 > 1$ is recovered asymptotically for sufficiently large radii. The crossover from the $T = 0$ result to the classical limit occurs when $k_B T \sim E_F(G_0/G)$, i.e., when the thermal energy $k_B T$ is comparable to the average transverse level spacing. Fig. 4(b) shows the stability diagram for $T/T_F = .05$, where $T_F = E_F/k_B$ is the Fermi temperature. One sees that the stability boundary indeed begins to cross over to the classical line $qR_0 = 1$ for $G_S > 20$.

In Fig. 4(b), there are no true metastable configurations with $G_S > 25 \sim T_F/T$, indicating that all thicker wires would be dynamically unstable (like a column of fluid) at this temperature, once the electronic shell effects have been smoothed out. However, $T_F = 3.75 \times 10^4$ K in sodium, so multistability from electronic shell effects can be expected to occur in sodium contacts with $G/G_0 \lesssim 125$ up to at least 300K.

Discussion

It should be pointed out that thermal averaging is not the only mechanism which can suppress electronic shell effects. Disorder also tends to smooth out the sharply peaked structure in the density of states, so that one can expect a reduction of shell effects when the diameter of the wire exceeds the mean free path. Furthermore, the tendency of the positive ions to order themselves into

regular arrays [19] will certainly affect the stability of metallic nanowires. Indeed, pioneering theoretical investigations [6–8] of the dynamics of nanowires focused exclusively on the arrangement of the ions. Based on the relative importance of electronic shells and crystal structure in metal clusters [4], one would expect electronic shell effects to dominate the energetics of very thin wires, particularly in the alkali metals, with crystal structure becoming increasingly important for thicker wires, and for metals where the bonding is more directional.

Although gold nanowires do not exhibit the sequence of magic numbers predicted here and observed in alkali metals, there is some evidence that gold nanowires can otherwise be adequately described using the free electron model [11,28,30]. It is thus worthwhile to speculate about a possible electronic origin for the remarkable stability of wires of individual gold atoms. Linear chains composed of four to seven gold atoms suspended between two gold electrodes, with a conductance $G = G_0$, were found to be stable in the laboratory for hours at a time [20,21]. Given that such a configuration has an enormous surface energy, its stability is at first sight surprising. However, in our free electron model, we find that an infinitely long wire with a conductance of G_0 is indeed stable with respect to small perturbations. Stable cylindrical gold wires with larger radii have also been observed recently [19].

Finally, let us comment on the dynamical evolution of a nanowire under elongation or compression. Consider stretching a nanowire that is initially in a stable configuration (white areas in Fig. 4). Under elongation, the radius of the wire decreases, so that one moves downward on the stability diagram. When a stability boundary is encountered, it becomes energetically (and dynamically) favorable for the wire to deform spontaneously, until another stable configuration of smaller radius is reached, thus causing the conductance to jump abruptly from one magic number to a smaller one, and conversely under compression. This scenario is consistent with the claim [18] that the structure of a metallic nanowire undergoes a sequence of abrupt changes as a function of elongation or compression. The finite widths of the unstable tongues in Fig. 4 also provides a possible explanation for the hysteresis [18] observed in the conductance as a function of elongation: the critical radius at which the wire's conductance jumps between neighboring magic numbers is different, depending on whether the tongue is approached from above or below, i.e., depending on whether the wire is stretched or compressed.

We thank J. M. van Ruitenbeek for useful discussions. F.K. was supported by Grant SFB 276 of the Deutsche Forschungsgemeinschaft, C.A.S. by NSF Grant DMR0072703, and R.E.G. by NSF Grant DMR9812526. This research was supported by an award from Research Corporation.

[1] Plateau, J. (1873) *Statique expérimentale et théorique des liquides soumis aux seules forces moléculaires*, (Gautier-Villars, Paris).

[2] Chandrasekhar, S. (1981) *Hydrodynamic and Hydromagnetic Stability* (Dover, New York), pp. 515-574.

[3] Brack M. & Bhaduri, R. K. (1997) *Semiclassical Physics* (Addison-Wesley, Reading, MA).

[4] de Heer, W. A. (1993) *Rev. Mod. Phys.* **65**, 611-676.

[5] Yanson, A. I., Yanson, I. K. & van Ruitenbeek, J. M. (1999) *Nature* **400**, 144-146.

[6] Landman, U., Luedtke, W. D., Burnham, N. A. & Colton, R. J. (1990) *Science* **248**, 454-461.

[7] Todorov, T. N. & Sutton, A. P. (1993) *Phys. Rev. Lett.* **70**, 2138-2141.

[8] Sørensen, M. R., Brandbyge, M. & Jacobsen, K. W. (1998) *Phys. Rev. B* **57**, 3283-3294.

[9] Krans, J. M., van Ruitenbeek, J. M., Fisun, V. V., Yanson, I. K. & de Jongh, L. J. (1995) *Nature* **375**, 767-769.

[10] Ashcroft, N. W. & Mermin, N. D. (1976) *Solid State Physics* (Saunders College Publishing, New York), pp. 29-55.

[11] Stafford, C. A., Baeriswyl, D. & Bürki, J. (1997) *Phys. Rev. Lett.* **79**, 2863-2866.

[12] Höppler, C. & Zwerger, W. (1999) *Phys. Rev. B* **59**, R7849-R7851.

[13] Stafford, C. A., Kassubek, F., Bürki, J. & Grabert, H. (1999) *Phys. Rev. Lett.* **83**, 4836-4839.

[14] Balian, R. & Bloch, C. (1970) *Ann. Phys. (N.Y.)* **60**, 401-447.

[15] Duplantier, B., Goldstein, R. E., Romero-Rochín, V. & Pesci, A. I. (1990) *Phys. Rev. Lett.* **65**, 508-511.

[16] D'Evelyn M. P. & Rice, S. A. (1983) *J. Chem. Phys.* **78**, 5225-5249.

[17] Ebner C. & Saam, W. F. (1975) *Phys. Rev. B* **12**, 923-939.

[18] Rubio, G., Agrait, N. & Vieira, S. (1996) *Phys. Rev. Lett.* **76**, 2302-2305.

[19] Kondo Y. & Takayanagi, K. (1997) *Phys. Rev. Lett.* **79**, 3455-3458.

[20] Ohnishi, H., Kondo, Y. & Takayanagi, K. (1999) *Nature* **395**, 780-783.

[21] Yanson, A. I., Rubio Bollinger, G., van den Brom, H. E., Agrait, N. & van Ruitenbeek, J. M. (1999) *Nature* **395**, 783-785.

[22] Creagh S. C. & Littlejohn, R. G. (1991) *Phys. Rev. A* **44**, 836-850.

[23] Ulmo, D., Grinberg, M. & Tomsovic, S. (1996) *Phys. Rev. E* **54**, 136-152.

[24] Creagh, S. C. (1996) *Ann. Phys. (N.Y.)* **248**, 60-94.

[25] Torres, J. A., Pascual, J. I. & Sáenz, J. J. (1994) *Phys. Rev. B* **49**, 16581-16584.

[26] Yannouleas C. & Landman, U. (1997) *J. Phys. Chem. B* **101**, 5780-5783.

[27] Zabala, N., Puska, M. J. & Nieminen, R. M. (1999) *Phys. Rev. B* **59**, 12652-12660.

[28] Bürki, J., Stafford, C. A., Zotos, X. & Baeriswyl, D. (1999) *Phys. Rev. B* **60**, 5000-5008.

[29] After completion of this work, we became aware of additional relevant experimental results and a novel data analysis by Yanson, A. I., Yanson, I. K. & van Ruitenbeek, J. M. (unpublished) cond-mat/0005157.

[30] Bürki J. & Stafford, C. A. (1999) *Phys. Rev. Lett.* **83**, 3342.